Infrared Physics & Technology 72 (2015) 19–28

Contents lists available at ScienceDirect

Infrared Physics & Technology

journal homepage: www.elsevier.com/locate/infrared

Extended hidden Markov model for optimized segmentation of breast thermography images

E. Mahmoudzadeh, M.A. Montazeri *, M. Zekri, S. Sadri

Department of Electrical and Computer Engineering, Isfahan University of Technology, Isfahan 84156-83111, Iran

HIGHLIGHTS

- Method can handle random sampling of images with re-estimation of model parameters.
- Run time is reduced in comparison with other related methods.
- Results show power of presented method for determination of the hottest vessels.
- Method maps semi hot regions into distinct areas.
- This approach provides an optimized segmentation method.

ARTICLE INFO

Article history:
Received 9 February 2015
Available online 11 July 2015

Keywords:
Breast cancer
Hidden Markov model
Segmentation
Thermography

ABSTRACT

Breast cancer is the most commonly diagnosed form of cancer in women. Thermography has been shown to provide an efficient screening modality for detecting breast cancer as it is able to detect small tumors and hence can lead to earlier diagnosis. This paper presents a novel extended hidden Markov model (EHMM), for optimized segmentation of breast thermogram for more effective image interpretation and easier analysis of Infrared (IR) thermal patterns. Competitive advantage of EHMM method refers to handling random sampling of the breast IR images with re-estimation of the model parameters. The performance of the algorithm is illustrated by applying EHMM segmentation method on the images of IUT_OPTIC database and compared with previously related methods. Simulation results indicate the remarkable capabilities of the proposed approach. It is worth noting that the presented algorithm is able to map semi hot regions into distinct areas and extract the regions of breast thermal images significantly, while the execution time is reduced.

1. Introduction

The hypothesis of breast thermography has been proposed more than 50 years. It has a controversial history. In the beginning, the poorly calibrated infrared cameras were primitive and captured breast images with poor resolution. Recently, interest in thermography is increased because of the availability of both highly sensitive infrared cameras and advances in image processing techniques [1]. Thermography has been shown to be well suited for the task of detecting breast cancer [2–6], in particular when the tumor is in its early stages or in dense tissue [7,8]. Early detection of breast cancer is important as it significantly provides higher chances of survival [9] and in this respect infrared imaging outperforms the standard method of mammography which can detect tumors only once they exceed a certain size. Tumors that are small in size can be identified using thermography due to the high metabolic activity of cancer cells which leads to an increase in local temperature picked up by infrared [10]. This modality can detect skin temperature differences of as small as 0.025 °C [11]. In addition, breast thermography is a non-invasive test and is valuable for alerting the physician to changes that can indicate early stage of breast disease, and so it offers the opportunity of earlier detection of breast cancer in comparison with self-examination, doctor examination or mammography alone [12]. In brief, a quick review of 15 large scale studies from 1967 to 1998, breast thermography revealed an average sensitivity and specificity of 90%. The researchers summarized the study by stating that "the findings clearly support that early identification of women at high risk of breast cancer based on the objective thermal assessment of breast health results in a dramatic survival benefit" [13]. To be more specific, breast thermography is a non-radioactive, non-contact and non-invasive imaging technology that works under the laws of physics of thermodynamics and

* Corresponding author.
E-mail addresses: e.mahmoudzadeh@ec.iut.ac.ir (E. Mahmoudzadeh), montazeri@cc.iut.ac.ir (M.A. Montazeri), mzekri@cc.iut.ac.ir (M. Zekri), sadri@cc.iut.ac.ir (S. Sadri).

http://dx.doi.org/10.1016/j.infrared.2015.06.012
1350-4495/

electromagnetic energy. It is proved that thermography is valuable in almost every application that analysis of temperature function is important. Thermography captures the thermal patterns of the breast and its surrounding. The temperature differences detected by thermal patterns are very subtle and most of the time cannot be felt by touch. It is in essence similar to the common practice of taking a patient's body temperature as one of his or her vital signs and shows if there is a functional problem to be investigated more deeply. However, an increase of body temperature is often an early warning sign. Breast thermography investigates the signs that might be due to abnormal function or reaction of the breasts. Identifying the nature of these signs will give a better understanding of breast health. Breast thermography may be considering as yearly checkup test which tracks and monitors the function of the breasts. Accordingly, breast thermography can be used as a monitoring, early detection and prevention tool and shows abnormal breast function [14].

The crucial part of any breast thermography examination is the interpretation of the images. The interpreter has to analyze each IR image to determine abnormal thermal patterns. The results might be followed by other means of testing such as mammography, ultrasound or MRI to confirm the interpretation. On the other, breast thermography is not a standalone tool in the screening and diagnosis of breast cancer. Thermography detects the abnormal signs that mammography and other structural technologies are not able to handle the same task. In fact, breast thermography is specifically worthwhile during the early stages of fast tumor growth, which is not yet recognizable by mammography as thermography is a physiological test while mammography is an anatomical one [15]. However, when clinical examination, mammography, and IR images were combined, a sensitivity of 98% was achieved. Both IR imaging and mammography technologies are of the complimentary nature. Neither used alone is sufficient, but when combined, each may counteract the deficiencies of the other. A combination of clinical examination, mammography and IR imaging may provide the greatest potential for breast conservation and survival [13].

An automatic system for screening, diagnosis and analysis of the breast thermal images contains image acquisition, ROI extraction, segmentation, pattern recognition and finally interpretation of the images. In segmentation stage, the thermal information can be shown in a pseudo colored image where each color represents a specific range of temperature [16]. Specially, the body temperature captured by IR camera is approximately in range of 27–34 centigrade degrees. Usually this tiny range of temperature is mapped to a large range from 0 to 255 in the breast thermography image and then the intensity image is quantized to reduce number of levels. Consequently, the segmentation provides a few regions in the output image which can be interpreted more easily.

Image segmentation techniques can play an important role to segment and extract these regions in the breast infrared images. Shape, size and borders of the hottest regions of the images can help to determine features which are used to detect abnormalities. For example it can determine how serious the tumor is and classifies its type. Unlike benign growth tumor which is encapsulated and has a smooth boundary, malignant tumor has an irregular shape. These facts help to distinguish the type of detected tumor from thermal image but it requires an accurate regional division [16]. Various methods can be applied to extract hot regions for detecting abnormal regions of interest in the breast infrared images and are presented in [16–20]. Also in the last six decades, many different image processing algorithms have been applied for image segmentation through image quantization such as Lloyd–Max, K-means, Fuzzy C-means and hidden Markov model. Among them, the hidden Markov model is a statistical model with strong theoretical basis. It has been used for image segmentation [21–23], human action recognition [24], image classification [25,26], texture analysis [27], edge detection [28], object recognition [29], medical images [30–32] and so on. In medical image processing, HMM has been used for classification [30], segmentation of brain MR images [31] and denoising [32].

This paper presents a new extension of hidden Markov model for segmentation of breast thermogram. EHMM proposes a novel method in order to map (quantize) 256 intensity levels to a proper lower level, which acceptable results are achieved. The proposed algorithm not only has ability to map semi hot regions into distinct areas significantly, it is able to extract the hottest regions with the acceptable similarity and matching to their respective original images. In the proposed method, by using randomly down sampled with non-uniform distribution technique, faster convergence of the procedure is obtained. After all, removing half of the pixels of the input image leads to low accuracy. To compensate this problem, EHMM investigates a novel method in order to restore the model parameters based on the relation between two successive outputs of the model. We compare the performance of the proposed method with known image segmentation algorithms such as: K-means, Fuzzy C-means, Lloyd–Max, self-organizing map (SOM) and standard HMM. These six methods are tested for 140 images of IUT_OPTIC database. In an attempt to analyze the hottest regions between left and right breast, boundary detection of the breast thermal images is done and as a result, left and right breasts are separated from each other. Then, the six segmentation methods are applied for malignant and benign cases. The extracted regions of thermal breast images in the cases, are compared to the original images. According to the results, the presented approach is an accurate method to perform efficient regional division for all cases. In addition, for malignant case, it is able to extract almost exact shape of the hottest regions.

The main features of the proposed segmentation method in this work are:

- The method has the ability to handle random sampling of the images with re-estimation of the model parameters.
- The execution time is reduced in comparison with previously related methods, such as Fuzzy C-Means, SOM and standard HMM.
- The results of this investigation show the strength of EHMM for determination of exact border of the hottest regions in malignant cases.
- This method is able to map semi hot regions into distinct areas. As a matter of fact, an accurate regional division is achieved without any additional mapping the region into sub-regions.

This approach provides an optimized segmentation method according to the solution of the basic HMM problems, which are based on Viterbi and Baum–Welch algorithms.

This paper is organized as follows: A brief background of hidden Markov model is given in Section 2. Section 3, describes the procedure of proposed EHMM segmentation method. Also, in this section, proof of optimization of segmentation approach is discussed. In Section 4, two different examples: synthetic alphabets and breast thermal images, are provided to verify the performance and capability of the presented algorithm in comparison with five other related methods. Also, in this section seven evaluation measures are identified and compared with other segmentation algorithms. Finally, a brief conclusion is drawn in Section 5.

2. Hidden Markov model

Hidden Markov Model (HMM) is introduced by Baum et al. in late 1960s and early 1970s. Considering mathematical basis of

the model, it can be applied in a wide range of applications [33]. Accordingly, when the model is designed and applied properly, it works very well in several applications. HMM is a statistical model with strong theoretical basis. Hidden Markov model can be viewed as a Markov model whose states cannot be explicitly observed. In fact, each state has a probability distribution over the possible output tokens. Therefore the sequence of tokens generated by an HMM gives some information about the sequence of states. HMM can be described at each fixed time as being in one state. Let us denote the state at time t by q_t and observation sequence by O. The output is produced according to the probability functions of the observations. Observation of each state is selected among the set of M possible outputs. Then the model can transit from one state to another one (or itself) according to the probability of transition between states.

Consider the N state discrete model with M possible outputs. Formally, an HMM is defined by the following parameters:

1. finite set of N hidden states;
$$S = S_1;\ S_2;\ \ldots;\ S_N$$

2. Distinct observation symbols per state, can be seen as physical output of the system;
$$V = V_1, V_2, \ldots, V_M$$

3. The transition matrix 'A', representing the probability of going from state S_i to state S_j;
$$\mathrm{A} = \{a_{ij};\ j = 1, \ldots, N\}$$
$$a_{ij} = P[q_t = S_i \text{ and } q_{t+1} = S_j] \quad i,j = 1, \ldots, N$$
$$\text{with } a_{ij} \geqslant 0 \text{ and } \sum_{j=1}^{N} a_{ij} = 1$$

4. The initial state probability vector 'π', representing probabilities of initial states;
$$\pi = \{\pi_i\} \quad i = 1, \ldots, N$$
$$\pi_i = P[q_1 = S_i] \quad i = 1, \ldots, N$$
$$\text{with } \pi_i \geqslant 0 \text{ and } \sum_{i=1}^{N} \pi_i = 1$$

5. Observation symbol probability distribution matrix 'B', representing the probability of producing observation k at time t in state S_i;
$$\mathrm{B} = \{b_j(O_t)\} \quad O_t = k$$
$$b_j(O_t) = P[V_k \text{ at } t | q_t = S_j] \quad j = 1, 2, \ldots, N \quad k = 1, 2, \ldots, M$$

For convenience, we denote an HMM as a triplet $\lambda = (\mathrm{A};\ \mathrm{B};\ \pi)$. Given the observation sequence $O = O_1 O_2 \ldots O_T$ and state sequence $Q = q_1 q_2 \ldots q_T$, $P(O, Q|\lambda)$ is calculated as follows.

$$\begin{aligned} &P(O,Q|\lambda) = P(O|Q,\lambda)P(Q|\lambda) \\ &P(O|Q,\lambda) = b_{q_1}(O_1)b_{q_2}(O_2)\ldots b_{q_T}(O_T) \\ &P(Q|\lambda) = \pi_{q_1} a_{q_1 q_2} a_{q_2 q_3} \ldots a_{q_{T-1} q_T} \\ &P(O,Q|\lambda) = \pi_{q_1} b_{q_1}(O_1) a_{q_1 q_2} b_{q_2}(O_2) \ldots a_{q_{T-1} q_T} b_{q_T}(O_T) \end{aligned} \tag{1}$$

Given an HMM with parameter set $\lambda = (\mathrm{A};\ \mathrm{B};\ \pi)$, three basic problems of interest must be solved for the model in order to be useful in real world applications. In [33], formal mathematical solution to these problems is presented. First, forward or backward algorithm is applied to calculate the probability of the observation sequence given the model; $P(O|\lambda)$. Viterbi algorithm is designed to solve second problem, namely finding the best state sequence associated with the given observation sequence and the model λ. The third basic problem of HMM is to determine a method for adjusting the model parameters (A; B; π) to maximize the probability of the observation sequence given the model. To this end, Baum Welch algorithm has been designed to solve the problem. The proposed method based on HMM is covered in the next section.

3. The proposed method

In an attempt to make thermal patterns findings from breast thermography image, we apply presented image segmentation algorithm. As a matter of fact, the temperature captured from IR camera is approximately in range of 27-34 centigrade degrees and this result is mapped to a range from 0 to 255. Accordingly, it is required to reduce the number of pixel intensity levels. In the other words, image quantization can be used to decrease the complexity of the image analysis. To this end, we should decrease 256 intensity levels to a proper lower level. In this work, with 8 quantization levels, acceptable results are achieved. In fact, the breast thermal image can be shown in a segmented image, where each region represents a specific range of temperature. In this way, hot regions are extracted and consequently important features such as shape, size and borders of them, can be used for abnormal patterns detection.

Considering the advantages of HMM mentioned in Section 2, we propose a novel extension of hidden Markov model in order to segment breast thermography images. In EHMM, using down sampling technique, the algorithm converges reasonably fast. In order to compensate low accuracy caused by removing half of the pixels, this work proposes a novel method for restoring the model parameters. The restoration is done according to the relation between two consecutive model outputs. In the following, we explain EHMM segmentation method and proof of optimization of the proposed approach.

At first, we define HMM parameters $\lambda = (\mathrm{A};\ \mathrm{B};\ \pi)$. Accordingly, the number of distinct observations, M, is set to 256, that is 256 levels for pixel intensities. The number of hidden states, N, is set to 8, that is 8 quantization levels as shown in Fig. 1.

Once the number of hidden states, N, and the set of possible observations for each state, M, were determined, matrix A, with size $N \times N$, and vector π, with size $1 \times N$, are initialized randomly. Then, Matrix B should also be set. We use supervised initialization for faster convergence of the algorithm. For this purpose we make use of Lloyd–Max quantization algorithm for the initialization. Thus each determined region quantized by Lloyd–Max algorithm is selected to be as initial region. After that, the histogram of pixel intensities for each level is set as initial values for matrix B.

In order to achieve faster convergence times, the image is randomly down sampled with non-uniform distribution by a factor of 2 before the observation sequence is calculated. After that, this down sampled image is an input for training step and we refer to this down sampled image as an image in the rest of the paper.

Considering the above explanations, the input image first is seen as a set of observation sequence with size of T ($T = W_1 \times W_2$, where W_1 is the number of rows and W_2 is the number of columns). Values of each element of the observation sequence is in range of 0–255.

Given the observation sequence $O = O_1 O_2 \ldots O_T$ and the initial model parameters $\lambda = (\mathrm{A};\ \mathrm{B};\ \pi)$, the training of the model is usually performed using the standard Baum–Welch re-estimation algorithm [33], which determines the parameters $\lambda = (\mathrm{A};\ \mathrm{B};\ \pi)$ that maximize the probability $P(O|\lambda)$. The computation of the

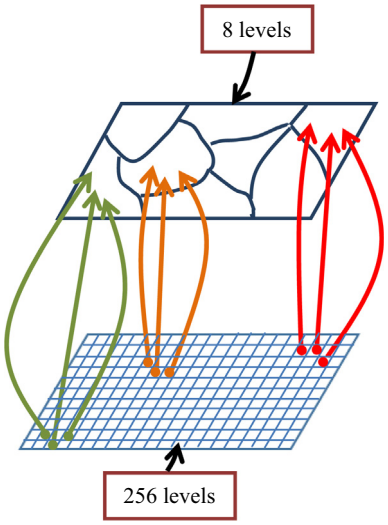

Fig. 1. Pixel mapping to 8 levels for image segmentation.

probability $P(O|\lambda)$, given a model λ and a new observation sequence O, is performed using the standard forward–backward procedure [33].

Faster convergence of the training procedure is obtained by using randomly down sampled with non-uniform distribution technique. After all, removing half of the pixels of the input image leads to low accuracy. To compensate this problem we investigate a novel method in order to restore the matrix A. Suppose that circles in Fig. 2 are hidden states and squares are observations at the time denoted by t:

The calculation of $P(O, Q|\lambda)$ is presented in (2) and (3), before and after down sampling respectively:

$$P(O,Q|\lambda) = \pi_{q_1} b_{q_1}(O_1) a_{q_1 q_2} b_{q_2}(O_2) a_{q_2 q_3} b_{q_3}(O_3) \ldots \quad (2)$$

$$P(O',Q'|\lambda) = \pi_{q'_1} b_{q'_1}(O'_1) a_{q'_1 q'_2} b_{q'_2}(O'_2) \ldots \quad (3)$$

It is obvious from Fig. 2 that

$$q'_1 = q_1, q'_2 = q_3$$

$$q'_{t'} = q_t \text{ with } t = 2 \times t' - 1,$$

Therefore, (3) is rewritten in the form of (4).

$$P(O',Q'|\lambda) = \pi_{q_1} b_{q_1}(O_1) a_{q_1 q_3} b_{q_3}(O_3) \quad (4)$$

We suppose that $P(O, Q|\lambda) \approx P(O', Q'|\lambda)$. Then by comparing (2) with (4), (5) is achieved.

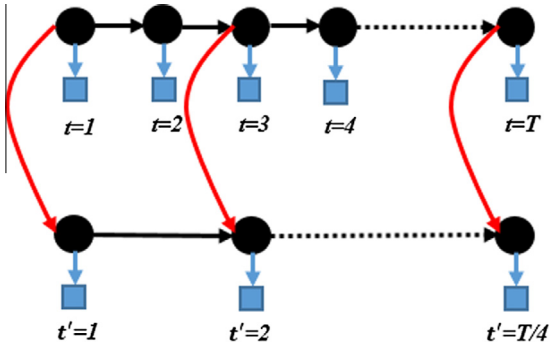

Fig. 2. Top: HMM shown with states and the observations before down sampling, Bottom: HMM shown with states and the observations after down sampling by a factor of 2.

$$a_{q_1 q_3} = a_{q_1 q_2} b_{q_2}(O_2) a_{q_2 q_3} \quad (5)$$

Since two neighbor pixels in the image do not have high intensity differences (except the edges), in (5), we consider $O'_2 \approx O_2$. Hence the general form of (5) can be written as (6).

$$a_{ij} = \sum_{k=1}^{N} a_{ik} a_{kj} b_k(O_t) \quad (6)$$

In order to restore the transition matrix A, the update process of (6) is carried out and matrix A is updated after completion of the training procedure and the algorithm convergence. As a matter of fact, the restoration is done according to the relation between two successive model outputs.

After training the model and obtaining the optimized parameters A, B and π, the quantization phase is executed by applying Viterbi algorithm. Consequently, the main image is converted to an image with only 8 quantization levels. Each region of the output image is due to a specific level. In the following, the proof of optimization of the proposed segmentation method is given.

Proof of optimization. As discussed before, Baum–Welch algorithm is used for training in the presented approach. If we define the current model as $\lambda = (A; B; \pi)$ and the re-estimated model as $\bar{\lambda} = (\bar{A}; \bar{B}; \bar{\pi})$, then it has been proven by Baum et all [33] that either (1) the initial model λ defines a critical point of the likelihood function, in which case $\lambda = \bar{\lambda}$; or (2) model $\bar{\lambda}$ is more likely than model λ, in the sense that $P(O|\bar{\lambda}) \geqslant P(O|\lambda)$, i.e., we have found a new model $\bar{\lambda}$ from which the observation sequence is more likely to have been produced [33]. Based on the above explanation, if we iteratively use $\bar{\lambda}$ in place of λ and repeat the re-estimation procedure, we have improved the probability of observation sequence being observed from the model.

After training stage, the input image is quantized by Viterbi algorithm and as a result each pixel is assigned to specific cluster (or region). The Viterbi algorithm is an approach for finding the most likely sequence of hidden states. It returns the state path that has the highest probability of generating a given sequence [34]. Note that the maximally likely path is not the only possible optimality criterion, for example choosing the most likely state at any given time requires a different algorithm and can give a slightly different result. But the overall most likely path provided by the Viterbi algorithm provides an optimal state sequence for many purposes [35].

4. Simulation results and discussion

For our experimental evaluation, we used a PC with Intel (R) Core (TM) i-5 3337U CPU 1.8 GHz and 4 GB RAM. The proposed method were realized by MATLAB 2010. In this section, two examples are given to demonstrate the validity of the proposed method and the segmentation results are compared with K-means, Fuzzy C-means, Lloyd–Max, self-organizing map (SOM) and standard HMM algorithms. In the first example, the objective is to show the ability of the presented segmentation approach on two synthetic images contain distinct and overlapped alphabets. In the second example, this method is applied on breast thermography images and segmentation results are compared and discussed for malignant and benign cases.

Example A. Synthetic images

This example presents a qualitative analysis in order to demonstrate the success and power of the method by two cases. In cases 1 and 2, the extraction of distinct and overlapped alphabets are considered respectively. At first, the two images are blurred by

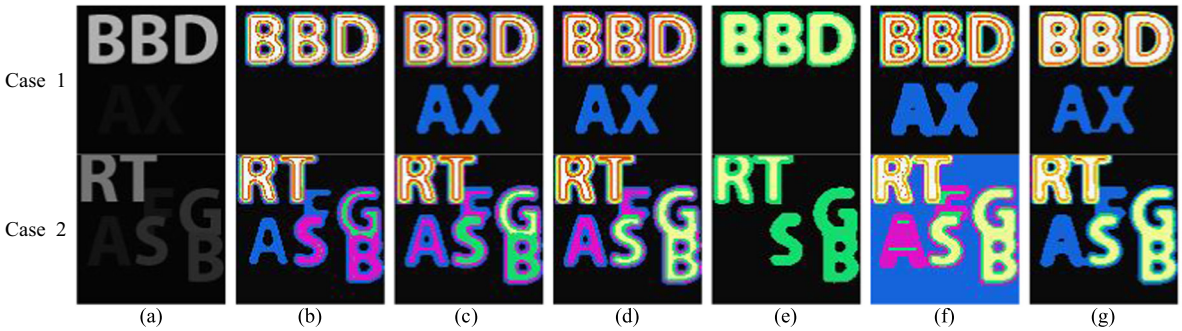

Fig. 3. (a) Alphabet synthetic images; (b) segmented image using Lloyd–Max; (c) segmented image using K-means; (d) segmented image using Fuzzy C-means; (e) segmented image using SOM; (f) segmented image using standard HMM; (g) segmented image using EHMM approach.

averaging window 5×5. A segmented algorithm should map the alphabets with equal level to a distinct level. The quantized image made by EHMM approach, shown in Fig. 3(g), is compared with the results of other known segmentation methods such as Lloyd–Max, K-means, Fuzzy C-means, SOM and standard HMM and are shown in Fig. 3(b)–(f) respectively.

Case 1 (distinct alphabets):

The first synthetic picture contained alphabets 'B' and 'D' with gray level of 180. Also 'A' and 'X' have gray level of 15. Alphabets in the images are poorly extracted using Lloyd–Max, K-means, Fuzzy C-means, SOM and standard HMM algorithms and the result is not acceptable. For example, the letter 'B' in the top row of Fig. 3(a), is not recognized well by Lloyd–Max, K-means, Fuzzy C-means and standard HMM algorithms and horizontal line in the alphabet is badly affected. As it is obvious from the top row of Fig. 3(g), this problem does not appear in the result of the proposed approach. Especially, it is clear from top row of Fig. 3(a), that alphabets with the level intensities close to the background intensity level are not determined by Lloyd–Max and SOM approaches.

Case 2 (overlapped alphabets):

The second synthetic picture contained alphabets 'R' and 'T' with gray level of 115. Also 'S', 'G' and 'B' have gray level of 45 and 'A' and 'F' are with gray level of 20. In this case, 'F' and 'S' with different gray levels and also 'G' and 'B' with the same gray level, are overlapped.

Similar to case 1, it is clear from the bottom image of Fig. 3(a), that alphabets with the level intensities close to the background intensity level are not determined by SOM approach. It worth noting that the presented segmentation method has efficiently mapped the alphabets 'S', 'G' and 'B' with equal level, to one region. In this case, there is a drawback of segmentation by K-means and Lloyd–Max. Also, letter 'A' and 'F' are not extracted well by K-means, SOM and standard HMM algorithms.

On the other, the overlapped alphabets with the same gray level ('S' and 'B') are properly clarified using EHMM method. In addition, in comparison with other methods, our algorithm is able to distinguish the borders properly. Furthermore, for overlapped alphabets with different gray levels ('S' and 'F'), only the presented work determines the alphabets accurately. Especially for closed alphabets such as 'F' and 'T', our method has an efficient ability to separate each letter.

In brief, it is clear that the alphabets are extracted sufficiently by the presented approach which determines all alphabets (not like Lloyd–Max and SOM) and without destroying the letters (as in Lloyd–Max, K-means, Fuzzy C-means and standard HMM).

Example B. Breast thermography images

In this work, we apply the proposed method for segmentation of breast thermography images of IUT_OPTIC database. First, screening standards for image acquisition are explained. Continuously, we try to show the capability of the presented algorithm for segmentation of malignant and benign cases in comparison with Lloyd–Max, SOM, standard HMM, Fuzzy C-means and K-means algorithms. In addition, we show that, the hottest regions extracted by the proposed method have at most perfect matching to their respective original images. Furthermore, in this case seven evaluation measures are identified in order to show the capability of the presented study quantitatively.

B.1 IUT OPTIC database

This study employs a collection of breast thermography images taken at JAM digital medical imaging center (an advanced laboratory with over ten years of experience in medical image acquisition and analysis). This database includes 160 breast thermal images from different views of the breast taken under the same environmental standard conditions. In addition, in this database, each patient has a thermography report that is confirmed by the skilled specialist. To this end, we designed the patient data form to cover the patient areas of complaints with specific healthy information, previous tests and examinations. In the form, any past histories of diagnoses and surgeries are to be documented for better understanding of the patient background.

In order to produce diagnostic quality infrared images, certain laboratory and patient preparation protocols stated in [36] was strictly adhered to. Consequently, we have considered the following standards for image acquisition and database production:

1. The imaging room must be temperature and humidity-controlled and maintained between 18 and 23 °C and kept to within 1 °C of change during the examination.
2. The room should also be free from drafts and infrared sources of heat (i.e., sunlight and incandescent lighting).
3. In order to properly prepare the patient for imaging, the patient should be instructed to refrain from sun exposure, stimulation or treatment of the breasts, cosmetics, lotions, antiperspirants, deodorants, exercise, and bathing before the exam.

4. The patient must underwent 15 min of waist-up nude. Then the patient placed their hands on top of their head in order to facilitate an improved anatomic presentation of the breasts for imaging.

B.2 Results

According to the above mentioned information, this work is applied on breast thermal images. Accordingly, 20 images (13%) are considered in the training step, which the model is converged. Then test images contains other 140 (87%) images from the database.

In this study, five different segmentation algorithms: Lloyd–Max, K-means, Fuzzy C-means, SOM and standard HMM were applied on the images. Then, the extracted regions are compared with the original images. In Fig. 4 the results of segmentation on two examples of breast thermography images using the proposed algorithm and above mentioned methods are provided. In the segmented image, according to the regions temperature from high to low, the regions are shown with white, red, orange, yellow, green, purple, blue and black respectively. So the first and second hottest regions are given with white and red colors respectively.

As shown in Fig. 4(b) and (f), Lloyd–Max and SOM approach don't determine the hot regions properly. Also, as shown in Fig. 4(c) and (d), the hottest regions are not determined by both the K-means and fuzzy c-means implementation. In addition, it is obvious from Fig. 4(f) that the exact shape of borders is not achieved by standard HMM algorithm. It can be seen from Fig. 4(g) that the presented approach can determine the hottest regions of the thermal image successfully. In addition, the exact borders of the hottest regions are properly detected to determine some useful features. This is covered in Fig. 5 in more details.

As it can be seen in Fig. 4, none of the other segmentation methods can separate the first hottest regions from the second hottest regions. This is covered in Fig. 6 in more details.

Moreover, it can be seen in the Fig. 4(c), (d) and (f) that in segmented images using K-Means, Fuzzy C-means and standard HMM (only top image) methods, an extracted vessel is determined as multi regions (one region for the innermost pixels and others for the border), instead of one region. Consequently, this multi regions segmentation is useless for interpretation and only lead to more complexity. It is clear from Fig. 4(g), that the presented approach is able to extract vessel as one region.

As a result, the presented segmentation algorithm gives more accurate result for segmentation of IR images. It has preferable efficiency and accuracy. The hottest regions extracted by this method are more similar and have at most perfect matching to their respective original images.

To demonstrate the success of the EHMM algorithm for malignant and benign cases, Figs. 5 and 6 show the hottest regions extracted by our approach in comparison with the best other related algorithms in more details.

Fig. 5 shows a comparison of segmentation images between the presented method and standard HMM, for a malignant case in left breast. Also, in Fig. 6 segmentation results of K-means and presented approach are compared, which left breast is a malignant and right breast is a benign case. As shown in the figures, neither standard HMM nor K-means can determine the exact shape and borders of the hottest regions. On the other, as shown in Fig. 6, the proposed method can separate first hottest regions from second hottest regions and consequently mapped semi hot regions into distinct areas. This fact is useful for effective interpretation of the breast images.

Briefly, according to the results, EHMM method is an accurate approach and has the potential of competitive advantages as follows:

- The results of this investigation show the strength of EHMM for determination of exact border of the hottest regions in malignant cases.
- This method is able to map semi hot regions into distinct areas. As a matter of fact, an accurate regional division is achieved without any additional mapping the region into sub-regions.

In the training step, the procedure continues until the mean of eight variances (each variance refers to pixels mapped to one determined regions) does not change. So the execution time consists of training step and also quantization step in order to calculate the variance measure. In our simulation, the training algorithm converges on 20 breast thermography images and takes 267.52 s. In the other, CPU time for quantization is covered in Table 1. According to the execution time demonstrated in Table 1, and segmented images shown in Fig. 4, reducing execution time of the segmentation algorithm without destroying the results is the advantage of this work and can lead to a faster convergence

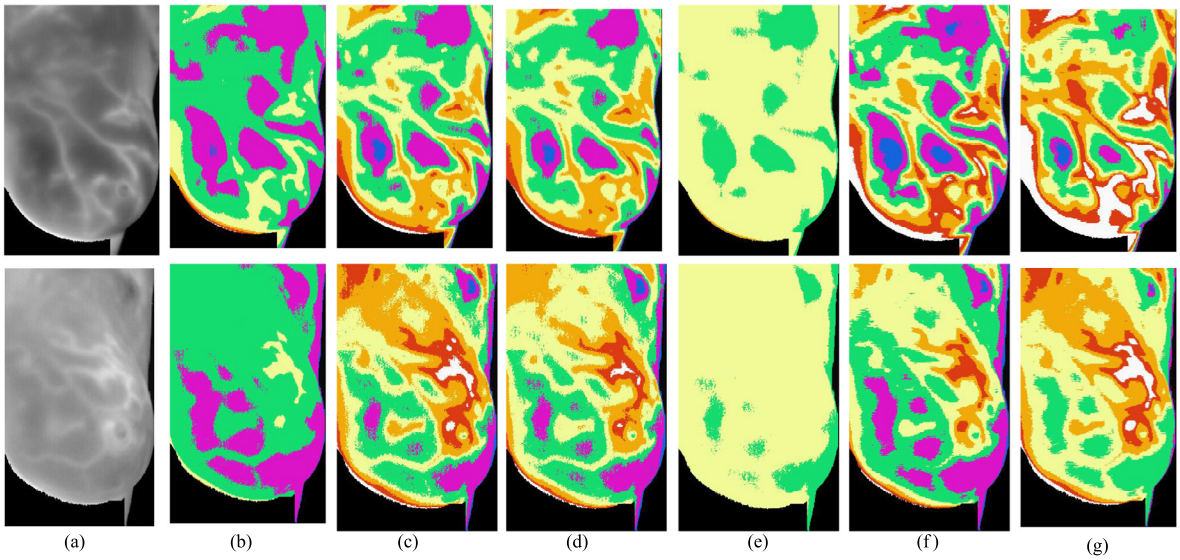

Fig. 4. (a) Breast thermography images of breast; (b) segmented image using Lloyd–Max; (c) segmented image using K-means; (d) segmented image using Fuzzy C-means; (e) segmented image using SOM; (f) segmented image using standard HMM; (g) segmented image using EHMM approach.

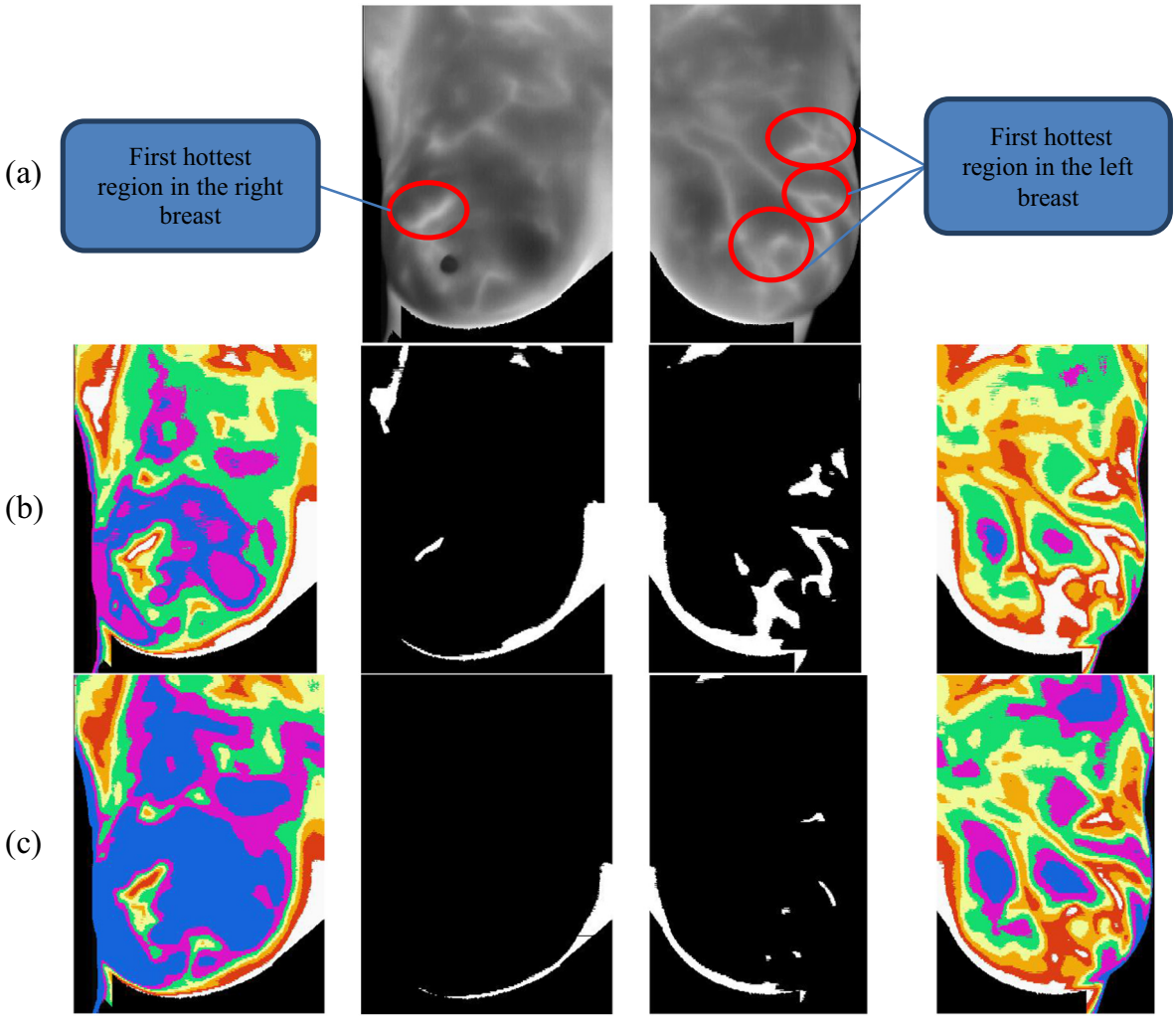

Fig. 5. (a) Original image, left breast is a malignant case, right breast is normal, (b) hottest regions extracted by EHMM method and (c) hottest regions extracted by standard HMM algorithm (the best other related algorithm for this image).

and accurate segmentation in comparison with the other related algorithms.

In order to quantitatively evaluate the presented method, two categories of measures are considered in the following.

B.3 Evaluation measures

In order to establish the proposed approach, its applicability is compared with five mentioned in the previous part, using some objective measures. These measures may be divided into two main categories: (1) One category consists of the whole segmented image; (2) another category assess the amount of the information of the pixels mapped to one determined region. The two measure categories are explained in the following.

1. ***The first category***

The assessment of the information in an image can be based on determining the amount of the information in the image either by the comparison of its histogram with the histogram of uniformly distributed image, or based on the pixel intensity distance with its neighbors in the segmented image. There are four definitions considering the above measures criterion following.

(a) For an image I, with the pixel intensity of r, the entropy of the probability function $p(r)$ is employed to quantify the amount of information in the image as in (7).

$$D_1(p) = -\sum_I p(I) \times \log(p(I)) \tag{7}$$

The information of the image increases as $D_1(p)$ is increased.

(b) The measure calculates the amount of realizable information in comparison with uniformly distributed image introduced in [37]. For this, the Kullback–Leibler (KL) Divergence is employed. In this context, digital image is modeled as discrete random field with a probability density functions. In KL algorithm, at first an image with "maximum realizable color information (MRCI)" is identified as in [37]. For grayscale images, we use maximum realizable information (MRI) instead of MRCI. Then the assessment of realizable information in an image can be based on comparison of its histogram $q(r)$ with the histogram $p(r)$ of the MRI image considered before. The Kullback–Leibler, or relative entropy divergence between the probability mass functions $p(r)$ and $q(r)$ is employed to quantify the similarity between

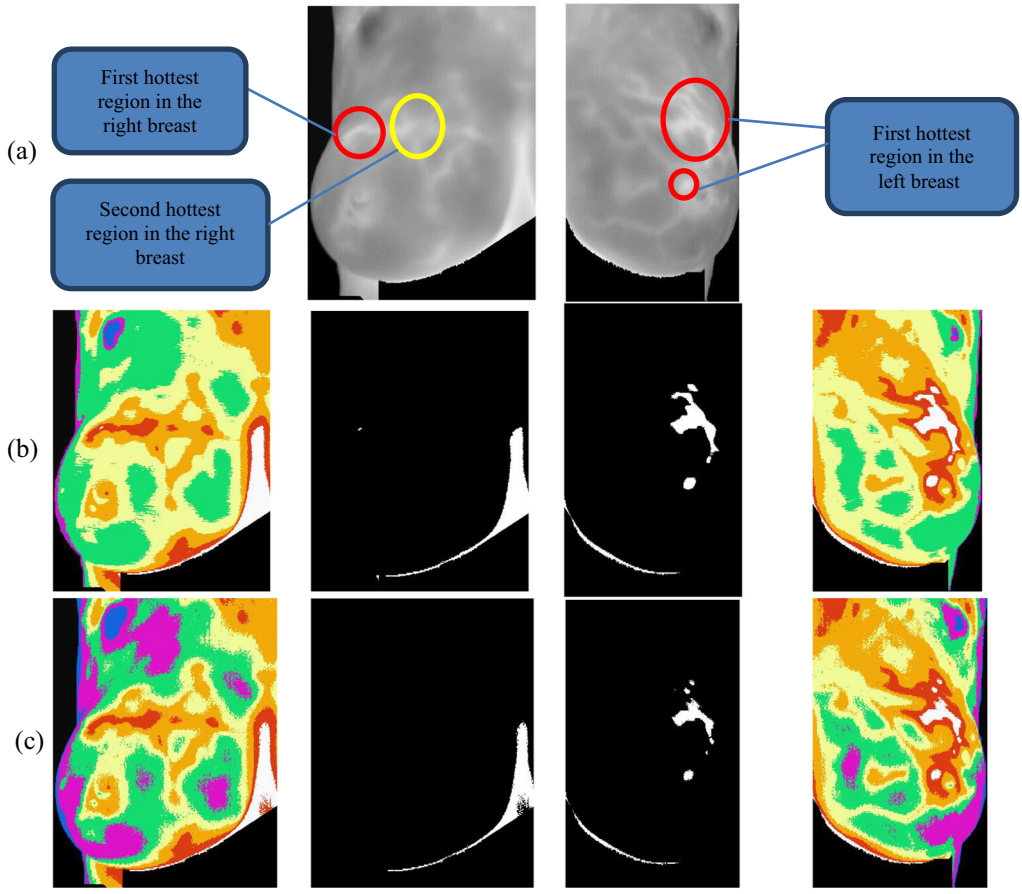

Fig. 6. (a) Original image, left breast is a malignant case, right breast is a benign case, (b) hottest regions extracted by EHMM method and (c) hottest regions extracted by K-means algorithm (the best other related algorithm for this image).

Table 1
Execution time for segmentation in second.

Algorithms	Execution time		
	Training for 20 images (s)	Testing for 140 images (s)	Average segmentation time (s)
Lloyd–Max	–	134.96	0.96
K-means	–	199.83	1.43
Fuzzy C-means	–	25,566	182.61
SOM	58.09	309,764	2213
Standard HMM	997.46	7.2625e+03	51.88
EHMM approach	267.52	2.6126e+03	18.66

$q(r)$ and $p(r)$ and consequentially between an image containing maximum realizable information (MRI) and the image under consideration. It is defined as (8).

$$D_2(p\|q) = \sum_I p(I) \times \log\left(\frac{p(I)}{q(I)}\right) \tag{8}$$

If $p(r)$ is close to $q(r)$, the quantity D_2 $(p||q)$ is close to zero, which means that the image with histogram $p(r)$ is almost ideal.

(c) The third measure uses the pixel intensity distance with its eight neighbors in the segmented image. For the distance, the second order gradient of the image is calculated using Laplacian operator as in (9):

$$D_3(f) = \left(\frac{1}{M \times N}\right) \times \sum_I \left(\frac{\partial^2 f}{\partial x^2} + \frac{\partial^2 f}{\partial y^2}\right) \tag{9}$$

In (9) the segmented image f has M rows and N columns. The higher value D_3, the higher information content of the image.

(d) The forth measure calculates the amount of realizable information with multiplying D_2 and inverse of D_3 as shown in (10).

$$D_4(f) = D_2(f) \times \left(\frac{1}{D_3(f)}\right) \tag{10}$$

The lower D_4, the higher information in the image f.

2. *The second category*

As mentioned before, the second category consists of the measures for assessing the information of the pixels mapped to one region. The calculation of the information of the pixels mapped to one region can be based on quantifying variance of pixels, or gradient of pixels, or the amount of information content of the pixels in one region. The segmented image f is considered as the union of all eight regions as in (11).

$$f = \cup_i R_i \tag{11}$$

In (11), R_i is a collection of pixels of region i after segmentation. In the second category, three definitions are given for the information content of the segmented image.

(a) The first measure, variance of pixels mapped to each region calculated and then average of all variances for the eight regions is obtained in (12).

Table 2
Measures calculated for segmented images produced by EHMM and other segmentation methods on 140 image.

Measure	Lloyd–Max	K-means	Fuzzy C-means	SOM	HMM	EHMM
D_1	0.56	**0.84**	**0.84**	0.30	0.80	0.79
D_2	0.64	**0.28**	**0.28**	1.00	0.29	**0.28**
D_3	**−0.02**	−0.03	−0.03	**−0.02**	−0.03	−0.03
D_4	−35.54	−8.56	−8.50	**−41.98**	−10.59	−10.21
D_5	41.55	34.39	**33.63**	117.11	70.82	80.46
D_6	−159.1	**−192.70**	−192.67	−79.70	−192.01	−170.76
D_7	0.93	1.08	1.09	**0.73**	1.11	1.11

$$D_5(f) = \left(\frac{1}{8}\right) \times \sum_i \text{variance}\ (R_i) \tag{12}$$

The lower average of variances of the pixels in eight regions and as a result the lower D_5, leads to more similarity between pixels mapped to one region and better segmentation.

(b) Another measure is based on definition of D_3 of the first category and is calculated as (13).

$$D_6(f) = \left(\frac{1}{8}\right) \times \sum_i D_3(R_i) \tag{13}$$

The lower value D_6, the lower average of gradient is obtained, which shows lower pixel intensity difference for the pixels mapped to each region, and consequently better segmentation is carried out.

(c) At last definition of D_1 is used as a measure for information content of the regions of segmented image as in (14).

$$D_7(f) = \left(\frac{1}{8}\right) \times \sum_i D_1(R_i) \tag{14}$$

The lower value D_7, the lower average for amount of information is obtained, and then the lower information value is calculated for the pixels mapped to one region, and consequently better segmentation is done.

All measures are calculated for the presented method and Lloyd–Max, K-means, Fuzzy C-Means, SOM and standard HMM algorithms for 140 images of database. Then the average of each measure for all images is obtained and is shown in Table 2. Number in bold font in Table 2 indicates the best segmentation result for each measure as has been explained in the related definition part.

It is obvious from Table 2, that in all measures the results of EHMM algorithm is comparable with other related segmentation methods. For measure D_5 the following explanations are required. In fact, one vessel should be set as one region but in the segmented image using other algorithms, is determined as multi regions. This caused to have low variance in each region and consequently, better value for D_5 is obtained. As mentioned in simulation results section, B.2 part, this multi regions segmentation is useless for interpretation and only lead to more complexity. It is clear that the presented approach is able to extract vessel as one region. Furthermore, this case is an advantage of EHMM method.

5. Conclusion

Breast cancer is one of the most common and dangerous cancers in women. Early detection of breast cancer is an important issue for cancer diagnosis. Thermography is a safe and non-invasive imaging modality and is a useful tool for detection of breast cancer cells in the early stages of disease progression. An automatic system for analysis of breast thermal images includes of boundary detection, segmentation, pattern recognition and finally interpretation of the images. As a result, a report should be generated for a patient which can accurately determine the abnormalities, which can help the physician for better diagnosis. In segmentation stage, the thermal image can be shown in an image where each intensity level represents a specific region. Consequently, the segmentation provides a few regions in the output image which can be interpreted more easily. In this work, we presented an extension of hidden Markov model for segmentation of breast thermography image. Importantly, the advantage of this method is that it is able to handle random sampling of the breast IR images with re-estimation of the model parameters. The results of comparisons show that execution time are efficiently reduced in comparison with Fuzzy C-Means, SOM and standard HMM algorithms and also EHMM method significantly improves the quality of the segmented images, compared with Lloyd–Max, K-means, Fuzzy C-Means, SOM and standard HMM algorithms. Planned future work includes analysis of the extracted abnormal regions obtained by the segmentation stage and accordingly, automatic interpretation of the images.

Conflict of interest

There is no conflict of interest.

Acknowledgements

Our most sincere thanks goes to Ms. Zahedi, Mr. Soltani and Mr. Razi for providing the images. We also like to appreciate the commitment and support of the staff member's of JAM Medical Imaging center, Isfahan, Iran.

References

[1] M. EtehadTavakol, E.Y.K. Ng, V. Chandran, H. Rabbani, Separable and non-separable discrete wavelet transform based texture features and image classification of breast thermograms, Infrared Phys. Technol. 61 (2013) 274–286.
[2] M. Milosevic, D. Jankovic, A. Peulic, Thermography based breast cancer detection using texture features and minimum variance quantization, EXCLI J. 13 (13) (2014) 1204–1215. ISSN 1611-2156.
[3] E.Y.K. Ng, L.N. Ung, F.C. Ng, L.S. Sim, Statistical analysis of healthy and malignant breast thermography, J. Med. Eng. Technol. 25 (6) (2001) 253–263.
[4] S.C. Fok, E.Y.K. Ng, G.L. Thimm, Developing case-based reasoning for discovery of breast cancer, J. Mech. Med. Biol. 3 (2003) 213–246.
[5] E.Y.K. Ng, S.C. Fok, Y.C. Peh, F.C. Ng, L.S.J. Sim, Computerized detection of breast cancer with artificial intelligence and thermograms, J. Med. Eng. Technol. 26 (4) (2002) 152–157.
[6] T.Z. Tan, C. Quek, G.S. Ng, E.Y.K. Ng, A novel cognitive interpretation of breast cancer thermography with complementary learning fuzzy neural memory structure, Expert Syst. Appl. 33 (2006) 652–666.
[7] N. Anbar, L. Milescu, A. Naumov, C. Brown, T. Button, C. Carly, K. AlDulaimi, Detection of cancerous breasts by dynamic area telethermometry, IEEE Eng. Med. Biol. Mag. 20 (5) (2001) 80–91.
[8] J. Head, F. Wang, C. Lipari, R. Elliott, The important role of infrared imaging in breast cancer, IEEE Eng. Med. Biol. Mag. 19 (2000) 52–57.
[9] M. Gautherie, Thermobiological assessment of benign and malignant breast diseases, Am. J. Obstet. Gynecol. 147 (8) (1983) 861–869.
[10] G. Schaefer, T. Nakashima, M. Zavisek, Analysis of breast thermograms based on statistical image features and hybrid fuzzy classification, LNCS 5538, Springer, 2008, pp. 753–762.
[11] W. Debi, K. Tina, Breast thermography history: theory and use, Nat. Med. J. 4 (2012).
[12] http://www.thermologyonline.org/Breast/breast_thermography_what.htm (visited 10.06.15).
[13] E.Y.K. Ng, A review of thermography as promising non-invasive detection modality for breast tumour, Int. J. Therm. Sci. 48 (5) (2009) 849–859.
[14] http://www.irinfo.org/articles/02-01-2013-james.html (visited 01.09.15).
[15] M. EtehadTavakol, E.Y.K. Ng, Breast thermography as a potential non-contact method in early detection of cancer: a review, J. Mech. Med. Biol. 13 (2) (2013) 1–20.
[16] M. Golestani, M. EtehadTavakol, E.Y.K. Ng, Level set method for segmentation of infrared breast thermograms, Exp. Clin. Sci. 13 (2014) 241–251. ISSN 1611-2156.

[17] M. EtehadTavakol, S. Sadri, E.Y.K. Ng, Application of K- and Fuzzy C-means for color segmentation of thermal infrared breast images, J. Med. Syst. 34 (2010) 35–42.
[18] E.Y.K. Ng, Y. Chen, Segmentation of breast thermogram: improved boundary detection with modified snake algorithm, J. Mech. Med. Biol. 6 (2) (2006) 123–136.
[19] X. Tang, H. Ding, Asymmetry analysis of breast thermograms with morphological image segmentation, Conference Proceedings of IEEE Engineering in Medicine and Biology Society, vol. 2, 2005, pp. 1680–1683.
[20] E.Y.K. Ng, Y. Chen, L.N. Ung, Computerized breast thermography: study of image segmentation and temperature cyclic variations, J. Med. Eng. Technol. 25 (2001) 1193–1200.
[21] K. Pyun, J. Lim, C.S. Won, R.M. Gray, Image segmentation using hidden Markov gauss mixture models, IEEE Trans. Image Process. 16 (7) (2007) 1902–1911.
[22] H. Choi, R.G. Baraniuk, Multiscale image segmentation using wavelet-domain hidden Markov models, IEEE Trans. Image Process. 10 (9) (2001) 1309–1321.
[23] A. Huang, R. Abugharbieh, R. Tam, Image segmentation using an efficient rotationally invariant 3D region-based hidden Markov model, In: Proceedings of the IEEE Computer Society Conference on Computer Vision and Pattern Recognition Workshops (CVPR'08), 2008, pp. 107–111.
[24] J. Yamato, J. Ohya, K. Ishii, Recognizing human action in time-sequential images using hidden Markov model, in: Proceedings of IEEE Conference on Computer Vision and Pattern Recognition, 1992, pp. 379–385.
[25] Jia. Li, Robert M. Gray, Richard A. Olshen, Multiresolution image classification by hierarchical modeling with two-dimensional hidden Markov models, IEEE Trans. Inf. Theory 46 (5) (2000) 1826–1841.
[26] J. Li, A. Najmi, R.M. Gray, Image classification by a two-dimensional hidden Markov model, IEEE Trans. Signal Process. 48 (2) (2000) 517–533.
[27] Guoliang Fan, Xiang-Gen Xia, Wavelet-based texture analysis and synthesis using hidden Markov models, IEEE Trans. Circuits Syst.—I: Fundam. Theory Appl. 50 (1) (2003) 106–120.
[28] Junxi Sun, Dongbing Gu, Yazhu Chen, Su Zhang, A multiscale edge detection algorithm based on wavelet domain vector hidden Markov tree model, Pattern Recogn. 37 (2004) 1315–1324.
[29] J. Hornegger, H. Niemann, D. Paulus, G. Schlottke, Object recognition using hidden Markov models, Pattern Recognit. Pract. IV 37–44 (1991).
[30] D. Keysers, C. Gollan, H. Ney, Classification of medical images using non-linear distortion models, in: Bildverarbeitung für die Medizin, Germany, 2004, pp. 366–370.
[31] Y. Zhang, M. Brady, S. Smith, Segmentation of brain MR images through a hidden Markov random field model and the expectation-maximization algorithm, IEEE Trans. Med. Imaging 20 (1) (2001) 45–57.
[32] Jixiang Zhang, Xiangling Zhang, Zhijun Pei, Medical image denoising using hierarchical hidden Markov model in the wavelet domain, First International Workshop on Education Technology and Computer Science, 2009.
[33] L.R. Rabiner, A tutorial on hidden Markov models and selected applications in speech recognition, Proc. IEEE 77 (2) (1989) 257–286.
[34] D. Golod, The *k*-best Paths in Hidden Markov Models. Algorithms and Applications to Transmembrane Protein Topology Recognition, University of Waterloo, Waterloo, Ontario, Canada, 2009.
[35] http://www.cs.cornell.edu/~ginsparg/physics/INFO295/vit.pdf (visited 15.06.15).
[36] J.D. Bronzino, Medical devices and systems, in: The Biomedical Engineering Handbook, third ed., CRC Press, Boca Raton, FL, Taylor & Francis, 2006.
[37] Vassilis Tsagaris, Vassilis Anastassopoulos, Assessing information content in color images, J. Electron. Imaging 14 (4) (2005).